Original article

Comparison of the accuracy of different handheld-type scanners in three-dimensional facial image recognition

Abbreviated title: Comparison of handheld-type scanners in three-dimensional facial image recognition

Authors

Yumi Tsuchida[a,b)], Maho Shiozawa[c)], Kazuyuki Handa[d)], Hidekazu Takahashi[e)], Hiroki Nikawa[b)]

[a)] Department of Digital Dentistry, Graduate School of Medical and Dental Sciences, Tokyo Medical and Dental University, Tokyo, Japan

[b)] Department of Oral Biology & Engineering, Graduate School of Biomedical and Health Sciences, Hiroshima University, Hiroshima, Japan

[c)] Department of Oral Prosthetic Engineering, Graduate School of Medical and Dental Sciences, Tokyo Medical and Dental University, Tokyo, Japan

[d)] Department of Advanced Prosthodontics, Graduate School of Medical and Dental Sciences, Tokyo Medical and Dental University, Tokyo, Japan

[e)] Course for Oral Health Engineering, Faculty of Dentistry, Tokyo Medical and Dental University, Tokyo, Japan

Comparison of the accuracy of different handheld-type scanners in three-dimensional facial image recognition

Abstract

Purpose: Handheld-type scanners are widely used in clinical practice. This study examined the accuracy of handheld-type scanners using plaster statues to assess their performance in facial recognition.

Methods: Twelve 4-mm zirconia balls as measuring points were attached to the facial portions of three types of plaster statue. Six digital facial images of each plaster statue were obtained using one of the following five handheld-type scanners: Artec Eva, Artec Spider, Bellus 3D FaceApp, SNAP, and Vectra H1. Four-millimeter spherical objects were manually placed at the measurement points on the scanned data generated using computer-aided design software and coordinate positions were measured using a contact-type high-resolution three-dimensional measurement device. Consequently, the discrepancy between the distance measured using the contact-type device and that measured using the handheld-type scanner was calculated. The scanning time, processing time, and deviation of the distance between the measuring points were analyzed using two-way analysis of variance and *t*-test with Bonferroni correction.

Results: The scanning and processing times ranged from 15.2 to 42.2 s and 20.7 to 234.2 s, respectively. Overall, 97% of all measured distances by Spider were within ±1.00% deviation; 79%, Vectra; 73%, Eva; 70%, Bellus; and 42%, SNAP.

Conclusions: The performance of handheld-type scanners using plaster statues varied among the different scanners. The scanning time of Eva and the processing time of Bellus were significantly shorter than those of other scanners. Furthermore, Spider exhibited the

best accuracy, followed by Eva, Vectra, Bellus, and SNAP.

Keywords

Facial imaging, handheld-type scanner, maxillofacial prosthesis, digital dentistry

1. Introduction

Acquiring facial shape information is important for prosthetic treatment. The facial characteristics are used as references for the occlusal plane. Furthermore, harmony between the prosthesis and the patient's mouth is crucial. Moreover, facial shape information is essential for the fabrication of maxillofacial prostheses and face shields in sports dentistry.

Facial shape is usually obtained using an alginate impression and plaster [1, 2], where impression material is placed on the entire face for a long time with breathing is allowed through a straw attached to the nose or mouth. However, this procedure is uncomfortable for patients with claustrophobia. Moreover, there is a risk of facial shape deformation during the impression-taking process owing to the weight of the materials [1, 3-5].

In recent years, studies have employed facial imaging data obtained using three-dimensional (3D) optical scanners in the field of dental treatment, such as maxillofacial prostheses, oral surgery, orthodontics, and cosmetic dentistry [6-11]. The application of a 3D optical scanner reduces patient discomfort during facial impression process.

Several types of 3D optical scanners are currently commercially available at various prices, performances, and sizes. The measurement principles for these products are based on laser scanning techniques, which are based on structured light [12]. Moreover, there are various concepts based on the shape and size of polygons that are used to reconstruct and create the surface structures of 3D images. The scanned data are usually output as a standard triangulated language (stl) or Wavefront obj file formats (obj). These can be integrated with other data such as dentition scanned using another device [9-11]. The stl file format comprises only one file of 3D geometrical data, whereas the obj file format comprise three types of files: 3D geometrical data (obj), texture data (such as jpg or png),

and information for combined data (mtl).

Most initial facial scanners were stand-type; however, handheld-type facial scanners have become popular owing to their ease of chairside use during dental treatment. Consequently, these handheld-type scanners are expected to be widely used in clinical practice. There have been several reports on the accuracy of facial imaging using handheld-type scanners. However, most of these studies examined human faces [13-17]. The shortcomings of these studies were the movement of the measuring points on the face, resulting in rough information on facial image deformation. Several studies have evaluated the distances between certain measuring points using a caliper; however, the measurement accuracy of the caliper is limited because of the minimum reading of the caliper and handling ability. Further, certain studies have evaluated the accuracy of facial imaging using the root mean square error or surface deviation color map of the models [15, 18-20]. In addition, the scanning accuracy should be considered in terms of trueness and precision. However, in previous studies investigating the scanning of human faces, the precision was evaluated, whereas trueness remained unclear.

The accuracy of different handheld-type scanners must be evaluated to identify an optimal handheld-type scanner for prosthetic treatment. Thus, the present study aimed to examine the accuracy of various handheld-type scanners using plaster statues to distinguish among their performances. The null hypothesis was that the performance of handheld-type scanners did not differ among the different products. In the present study, plaster statues were considered as scanning targets to avoid movement of the human face. Moreover, a coordinate measuring machine (CMM) was used to obtain more accurate measurements of the true values.

2. Materials and methods

2.1. Scanning targets

Three types of plaster statues (Agrippa [chamfered and half-face], Saint George, and Hermes; Sekaido, Tokyo, Japan) were used as scanning targets (Fig. 1). In the preliminary experiment, certain handheld-type scanners could not easily recognize the plaster statue without characterization of the human face; thus, the facial portion of the statues was characterized using a face foundation, eyebrow pencil, and eyeliner. Further, 12 measuring points of a 4-mm zirconia ball (YTZ-4, Nikkato, Osaka, Japan) were attached to the face of the statue, similar to previous reports (Fig. 2, Table 1) [14, 16, 17].

2.2. Scanners

Five handheld-type scanners were selected; two industrial 3D scanners (Artec Eva, Artec 3D, Luxembourg: Eva; Artec Spider, Artec 3D: Spider), two medical scanners for obtaining facial image (SNAP, DOF, Seoul, Korea: SNAP; Vectra H1, Canfield Scientific, New Jersey, US: Vectra), and one smartphone (iPhoneX, Apple, California, US) with an application for facial imaging (Bellus 3D FaceApp, Bellus3D, California, US: Bellus). The specifications of the devices used for the scanning are listed in Table 2.

2.3. Digital Impression

Six digital facial images of each plaster statue were obtained using each scanner according to the manufacturer's instructions. Consequently, 90 scanned images were acquired (three statues × five scanners × six scans). Scanning using Eva, Spider, and SNAP was started from the nose, shifted to the left cheek, and rotated several times in a clockwise direction until a complete image was obtained. Further, scanning using Bellus

started from the frontal face and then moved from the right face to the left face according to the manufacturer's instructions. Regarding Vectra, photographs of the face were captured from the front, lower right, and lower left. The scanned images were obtained in the same room by a single operator. Scanning using Eva and Spider was performed in the smooth fusion mode, which is suitable for scanning the human body because it can cancel for slight body movements during scanning. The resolutions, which refer to the minimum length of an edge per polygon, for Eva and Spider were 0.8 and 0.5 mm, respectively. Holes on the imaged surfaces smaller than 5 mm were filled automatically. Further, the size of the texture images was 4096 × 4096 pixels. For the other scanners, scanning was performed without modifying the setting conditions. The time required for obtaining facial data and processing it to construct facial images were recorded as the scanning and processing times, respectively. Scanned data were output in the obj file format as images (jpg or png) and mtl files. Subsequently. the average length of the extracted 30 sides of the polygon in the flat forehead area of each scanner's image was calculated.

2.4. Measuring surface deviation from high-precision scan data

A 3D high-precision optical scanner (ATOS CompactScan 2M, GOM, Niedersachsen, Germany; the distance between the measuring points was 0.075 mm) was used to scan the face of Hermes. 3D scanning software (Artec Studio 12 Professional, Artec) was used to superimpose the facial data of Hermes scanned by ATOS and five other models. After cropping the unwanted portions, the surface deviation color maps between the ATOS and each scanned data point were output.

2.5. Distance between measuring points

The data acquired by the handheld-type scanner were imported into 3D computer-aided design (CAD) software (Freeform, 3D systems, South Carolina, USA). Thereafter, 4-mm spherical objects were manually placed at the locations of the measurement points by a skilled dental technician. Shape and texture images were used as references to determine the locations of the measurement points. The center of the sphere was set to coincide as much as possible with that of the zirconia ball image, and the sphere did not penetrate into the scanned facial surface data. Subsequently, using the center coordinates of the spherical object, the distance from the nasion (NAS) to each measurement point was calculated using the following formula:

$$distance\ d_n\ =\ \sqrt{(x_0 - x_n)^2 + (y_0 - y_n)^2 + (z_0 - z_n)^2}$$

where, d_n is the distance from the measuring point of n. The coordinate values of the NAS were set to x_0, y_0, and z_0, and those of the measuring points were set to x_n, y_n, and z_n.

The coordinate positions of each measurement point were measured thrice using a CMM contact-type high-resolution 3D measurement device (QM-measure 353, Mitutoyo, Kanagawa, Japan). The error indicated by the CMM for size measurement (E) is defined as follows:

$$E\ =\ (3.0 + 4L/1000)\ \mu m$$

where, L is the measured distance.

The distance from the NAS to each measurement point measured using CMM was calculated as the true value of the measurement. The percentage discrepancies (Δd) between the distance between the measured value obtained using the handheld-type scanner and the true value were calculated using the following formula:

$$\Delta d = \frac{(d_n - d_r)}{d_r} \times 100$$

where d_n is the true value, and d_r is the distance measured with the handheld-type scanner.

The average of six discrepancies (Δd) and standard deviations between the measured values are referred to as "trueness" and "precision," respectively, in this study [21]. The trueness and precision values of 11 measuring points of three plaster statues for each handheld-type scanner were pooled, and the relationship between the length of polygons and the accuracy (trueness and precision) of the five scanners was evaluated.

2.6. Statistical analysis

Scanning and processing times were analyzed separately using two-way analysis of variance (ANOVA) and t-test with Bonferroni correction. Two factors were analyzed: scanners (Eva, Spider, Bellus, SNAP, and Vectra) and scanning targets (Agrippa, George, and Hermes).

Further, the discrepancies in the distance between measuring points on the Agrippa, George, and Hermes statues were analyzed separately using two-way ANOVA and t-test with Bonferroni correction. The two factors analyzed were scanners (Eva, Spider, Bellus, SNAP, and Vectra) and measuring points shown in Table 1 (TRI, PRN, SN, TUL, POG, RLC, LLC, RMC, LMC, RCH, and LCH).

The relationship between the length of polygons and trueness and that between the length of polygons and precision of the five hand-held type scanners were analyzed using Dunn's test with Bonferroni correction because homogeneity and normality were not accepted by the Leven and Shapiro-Wilk tests, respectively.

All analyses were performed using statistical software (SPSS version 24.0, IBM Corp., Armonk, NY, USA). The significance level was set at $p < 0.05$.

3. Results

3.1. Scanning time and processing time

The scanning and processing times ranged from 15.2 to 42.2 s and 20.7 to 234.2 s, respectively (Table 3). The two-way ANOVA of the scanning time suggested the statistical significance of the two main factors and their interactions. The scanning time using Eva was significantly shorter than those using the other scanners, whereas that using Spider was significantly longer than those using the other scanners. Further, the scanning times using Eva, Spider, and Bellus did not vary depending on the scanning targets. However, those using SNAP and Vectra varied depending on the scanning targets.

Furthermore, the processing time using Bellus was significantly shorter than that using the other scanners, and that using Spider was significantly longer than that using the other scanners. The processing time using Bellus and Vectra did not vary depending on the scanning targets; however, that using Eva, Spider, and SNAP varied depending on the scanning targets.

3.2. Digital impression image

Digital impression images of Hermes with and without the texture and close-up areas of the eye are shown in Figs. 3 and 4, respectively. The color, brightness, and resolution of the texture images differed among the capturing scanners. The images obtained using Spider were brighter and yellowish, and those obtained using Bellus and SNAP were darker. Further, the shapes of the zirconia balls generated without the texture using Eva,

Spider, and Vectra were clearly recognized, whereas those generated using Bellus and SNAP could not be recognized. In addition, the surfaces produced using Eva, Spider, and SNAP were relatively smooth, whereas those produced using Bellus and Vectra were relatively coarse. Moreover, the areas around the eyes scanned using SNAP were not clear; whereas, those generated using Bellus were deformed compared with those generated using the other scanners. The average lengths and standard deviations of the polygons of Eva, Spider, Bellus, SNAP, and Vectra were 0.83±0.21, 0.46±0.15, 2.10±0.70, 1.91±0.28, and 1.23±0.19 mm, respectively.

Typical surface deviation color maps of each scanner compared with high-precision scan data are shown in Fig. 5. The surface discrepancies of Spider were approximately within ±0.4 mm; those of Eva were similar to Spider except for measuring points whose deviations were smaller than 1.0 mm. Regarding Bellus and SNAP, the deviation around the area of crista nasalis and eyebrows were smaller than 0.6 mm, and, oral fissure and medial canthus were greater than 0.6 mm. Bellus and SNAP images had wider areas of discrepancy, particularly around the eyes and mouth.

3.3. Discrepancies between the measured values

Trueness of Eva, Spider, Bellus, SNAP, and Vectra ranged from -2.49 to 2.01, -1.03 to 0.56, -6.08 to 4.66, -6.44 to 4.66, and -3.93 to 0.87%, respectively (Table 4). Further, the precision of Eva, Spider, Bellus, SNAP, and Vectra ranged from 0.18 to 0.94, 0.05 to 0.56, 0.08 to 2.05, 0.20 to 1.87, and 0.14 to 1.27%, respectively. Two-way ANOVA results showed the statistical significance of the two main factors: the type of scanner and the measuring points, and their interaction. Regarding Bellus, SNAP, and Vectra, the discrepancies of the RMC and LMC for George and Hermes were greater than those for

Agrippa, indicating a shorter distance of RMC and LMC for George and Hermes than that for Agrippa; however, the other discrepancies did not exhibit obvious tendencies among the plaster statues. The percentage discrepancies of each handheld-type scanner are summarized in Table 5. All discrepancies of Spider, except for Hermes' TRI, were within ±1.00%; there were no significant differences among all measuring points, as shown by the t-test with Bonferroni correction. Discrepancies within ±1.00% of Vectra, Eva, and Bellus were 79, 73, and 70%, respectively, and that of SNAP was 42%. Furthermore, the distribution of discrepancies in Eva was small and within ±3.00%; those of Bellus and Vectra were skewed to a negative value, whereas that of SNAP was skewed to a positive value.

The relationship between the length of polygons and trueness and that between the length of polygons and precision of the five handheld-type scanners are shown using box-and-whisker plots in Figs. 6 and 7, respectively. The trueness of Spider (length of polygons was 0.46 mm) included 0.00% in the box. The median of the trueness of the other scanners did not change dramatically, but the whiskers showed a tendency of elongation with an increase in the length of the polygons. In contrast, the precision of Spider was the smallest, and the median and whiskers of the other scanners increased with an increase in the polygon length.

4. Discussion

The null hypothesis that the performance of handheld-type scanners did not differ among the different products was rejected.

There are variations among human faces; therefore, multiple target statues were used to evaluate faces with different expressions. The criteria for selecting scanning targets

were statues exposing both the ears and forehead area. Three statues with a simplified face (Agrippa), rather stern expression (George), and neutral expression (Hermes) were selected. Dimensional evaluation using the plaster statue was easier and more accurate than that using a human face because the measurement points did not move owing to changing facial expressions, and a high-precision contact measurement device could be applied. However, the plaster statue without coloring could not be scanned by Bellus because the color information of the scanning target could be employed to reconstruct the facial image. Therefore, all plaster statues were characterized before scanning. Regarding Bellus, SNAP, and Vectra, the RMC and LMC for George and Hermes were shorter than the true value; however, no other obvious tendency were found among the scanning targets. RMC and LMC are the points with the shortest distance from the NAS in all plaster statues. Therefore, the percentage of error for these points was calculated to be relatively large.

Facial impressions recorded using a facial scanner are less uncomfortable for the patient than those recorded using alginate or plaster. Furthermore, there was no deformation of the actual face owing to the weight of the impression material. The facial scanner can also obtain impressions with eyes open. In this study, the accuracies of two highly accurate industrial scanners, two medical scanners, and one smartphone with an application for facial imaging were evaluated. The industrial scanners used were not specialized for facial scanning but could be applied to scan various shapes and large-sized targets, whereas the medical scanners used were designed for facial image acquisition. The contact-type measurement device, which is considered reliable and highly accurate, was used to determine the true value of the coordinate positions of the measurement points. To visualize the deformation of the facial images obtained in this study, the

industrial scanner with high accuracy was used.

The measurement points on the targets were based on previous reports [14, 16, 17]. A previous study reported that plastic blocks could be attached to the measuring point for easier recognition [13]. Zirconia balls were attached for the same purpose in the present study. However, the spherical projections on the obtained 3D images were smaller and less clear than the original ball on the plaster statues. Therefore, the color information of the texture image was used to determine the locations of measurement points. However, the positions of the measurement points on the 3D image without texture did not always match those with texture, particularly when the deformation of the 3D image was large. The accuracy of the scanners in the present study was considered including this issue.

The scanning times of all scanners were within 42 s, which is an acceptable time for retaining the posture of a human being. Furthermore, the facial impression recorded using a handheld-type facial scanner required less time than that recorded using alginate and plaster because of their setting time. The processing time of Eva and Spider included times to superimpose the scanned data and to delete unnecessary areas, and that of Vectra included times to import data from the device to a personal computer. Moreover, the processing time was a reference value because it depends on the performance of the computer to control and process the device. In general, the processing time increases when the size of the polygon obtained is small.

Usually, in the facial impression method using alginate and plaster, the color information of the face must be obtained separately from the model as a photograph. However, all scanners used in this study could display face colors on 3D geometrical data. All scans were performed under room light, but the color of the face of the textures varied among the handheld-type scanners. This issue was considered because of the lightning

usage of the device and the distance between the target and the device. However, the colors of the face can be adjusted after scanning using image processing software because the texture data are saved separately from the 3D geometrical data.

The accuracy of facial images varied among handheld-type scanners. The reasons for these variations are considered to be the scanning principles, strategies, and algorithms for reconstructing scanning images used by the examined scanners. The size of the polygons varied from 0.46 to 2.10 mm depending on the scanners; but Eva and Spider could adjust the size of the polygons by changing the parameters when reconstructing the 3D shape. If the parameters were changed to reduce the polygon size, the processing time and data file size would be prolonged and larger, respectively. In this study, the manufacturer's recommended parameters for Eva and Spider were used because their polygon lengths were already smaller than those of the other scanners. The length of the polygons of each handheld-type scanner did not influence trueness, but influenced the precision of each scanner. When the length of the polygons increased, the shape of the measuring point became unclear; therefore, determination of the location of the measuring point was difficult, and the location of the measuring point could not be determined exactly apart from the measuring point. Consequently, precision was influenced by the length of the polygons, but trueness was not.

The surface deviation color maps of the high-precision scan data and scanned data were evaluated. There was no obvious difference among the six scans of each handheld-type scanner; a typical surface deviation color map is shown in Fig. 5. Regarding Bellus and SNAP, convex portions such as the crista nasalis and eyebrows were smaller and concave portions such as the oral fissure and medial canthus were larger. These findings were obtained because the greater length of polygons could not follow the acute

morphological change. Moreover, the reconstruction strategies and algorithms for reconstructing scanning images, such as using different patterns of polygon shapes (equilateral triangle or inequilateral triangle) (Fig. 4), might be responsible.

Furthermore, in this study, not only the surface deviation color maps but also the distances between the measuring points were calculated; therefore, it was possible to discuss the specific deformation of the facial image. The discrepancy between the mean and true values and the standard deviation of the measured distance in the present study corresponded to the trueness and precision, respectively. The true values were calculated using the high-precision contact-type measuring device with an error of indication of the CMM for a size measurement of less than 4.1 μm in the present study, which is more accurate than that reported in previous studies [13, 14, 16, 17]. Modabber et al. [13] and Franco de Sá Gomes et al. [17] reported that the trueness values ranged from 0.171 to 0.708 mm and from -4.65 to -0.89%, respectively in case of Eva. Regarding Vectra, Savoldeli et al. [16] reported that trueness ranged from -3.72 to 8.00%. These values were similar to those obtained in this study, suggesting that the results obtained are reliable.

According to the results of this study, the accuracies of the industrial scanners Eva and Spider were superior; however, they are expensive, and a wired connection with a computer is essential for their functioning. Moreover, Eva and Spider provide intense glare due to pattern projection, causing patients to close their eyes. In contrast, although the accuracies of the medical scanners in the present study were inferior, they were inexpensive compared to industrial scanners. The relationship between the accuracy and price of the handheld scanner is a trade-off.

The accuracy required to fabricate facial prostheses should be within 1.0 mm [5]. However, human skin is a nonlinear, anisotropic, and viscoelastic material [22], and is

therefore easily deformed. Furthermore, Holberg [1] reported that the average discrepancy between the plaster cast and facial surface was 2.3 mm when the facial impression was recorded using alginate and plaster. Consequently, an accuracy within 2.0 mm may be clinically acceptable for fabricating a facial model. If the tolerance was 1.0 mm, the accuracy of the Spider, Eva, and Vectra was clinically acceptable. Whereas, if the tolerance was 2.0 mm, the accuracy of Bellus was also acceptable, but that of SNAP was not acceptable because of great deformation in certain areas. Therefore, it is necessary to pay attention to obtain facial data using SNAP for certain areas, such as the lower mandible and medial canthus, as shown in Fig. 5. All scanners used in the present study provided photo-based textures, which were helpful in evaluating the geometrical data, although the photo-based texture was a two-dimensional image. Consequently, the accuracies of all scanners were considered to be within an acceptable range for clinical usage, but a specific portion of the image, such as around the eye, showed a relatively large deformation. Therefore, the handheld-type scanner should be selected based on the area of interest and the required image quality.

The purpose of this study was to evaluate the accuracy of handheld-type scanners for facial images; therefore, factors such as lighting, distance, angle, alignment of scanner and object, and operator were not considered. The effect of these scanning conditions on scanning accuracy will be investigated in future studies. In the present study, plaster statues were used as scanning targets to examine the scanning accuracy; however, actual human faces occasionally change, move, and deform with facial expressions and poses. It is necessary to confirm whether the results obtained in the present study are similar to those obtained in humans. Moreover, the plaster statues used in the present study had no facial defects; however, defects were present on the faces of patients requiring

maxillofacial prostheses or sports face shields in some cases. These issues should be addressed in future studies. The accuracy of the frontal face, excluding the ears, by handheld-type scanners was evaluated in the present study, but information, including the ears, is important for supporting a sports face shield. Therefore, it is necessary to evaluate the accuracy of scanning a wider frontal face area. In addition, new technologies for 3D reconstruction without a scanner, such as photogrammetry, are becoming popular. Therefore, the accuracy of 3D reconstruction using these technologies should be evaluated in the future.

5. Conclusion

To assess the performance of different handheld-type scanners, the accuracy of the five handheld-type scanners was examined using three plaster statues.

The scanning and processing times ranged from 15.2 to 42.2 s and 20.7 to 234.2 s, respectively. The scanning time using Eva ranged from 15.2 to 18.3 s, and the processing time using Bellus ranged from 20.7 to 23.5 s. These values are significantly shorter than those obtained using other scanners.

Overall, 97% of all distances measured by Spider were within ±1.00% deviation, 79% for Vectra, 73% for Eva, 70% for Bellus, and 42% for SNAP. The distribution of discrepancies in Eva was small (within ± 3.00 %).

Thus, the performance of handheld-type scanners using plaster statues varies among scanners. Spider had the best accuracy, followed by Eva, Vectra, Bellus, and SNAP.

Conflict of interest statement

Declarations of interest: none.

References

[1] Holberg C, Schwenzer K, Mahaini L, Rudzki-Janson I. Accuracy of facial plaster casts: A three-dimensional scanner study. Angle Orthod 2006;76:605-11. https://doi.org/10.1043/0003-3219(2006)076[0605:AOFPC]2.0.CO;2.

[2] Ueno T, Churei H. Fabrication technique for thermoforming material. Int J Sport Dent 2008;1:67-71.

[3] Runte C, Dirksen D, Deleré H, Thomas C, Runte B, Meyer U, et al. Optical data acquisition for computer-assisted design of facial prostheses. Int J Prosthodont 2002;15:129-32. https://doi.org/10.1016/j.jcms.2018.05.020.

[4] Reitemeier B, Notni G, Heinze M, Schöne C, Schmidt A, Fichtner D. Optical modeling of extraoral defects. J Prosthet Dent 2004;91:80-4. https://doi.org/10.1016/j.prosdent.2003.10.010.

[5] Matsuoka A, Yoshioka F, Ozawa S, Takebe J. Development of three-dimensional facial expression models using morphing methods for fabricating facial prostheses. J Prosthodont Res 2019;63:66-72. https://doi.org/10.1016/j.jpor.2018.08.003.

[6] Choi JW, Lee JY, Oh TS, Kwon SM, Yang SJ, Koh KS. Frontal soft tissue analysis using a 3 dimensional camera following two-jaw rotational orthognathic surgery in skeletal class III patients. J Craniomaxillofac Surg 2014;42:220-6. https://doi.org/10.1016/j.jcms.2013.05.004.

[7] Hanawa S, Kitaoka A, Koyama S, Sasaki K. Influence of maxillary obturator prostheses on facial morphology in patients with unilateral maxillary defects. J Prosthet Dent 2015;113:62-70. https://doi.org/10.1016/j.prosdent.2014.06.016.

[8] Mertens C, Wessel E, Berger M, Ristow O, Hoffmann J, Kansy K, et al. The value of

three-dimensional photogrammetry in isolated sagittal synostosis: Impact of age and surgical technique on intracranial volume and cephalic index─a retrospective cohort study. J Craniomaxillofac Surg 2017;45:2010-6. https://doi.org/10.1016/j.jcms.2017.09.019.

[9] Park JM, Oh KC, Shim JS. Integration of intraoral digital scans with a 3D facial scan for anterior tooth rehabilitation. J Prosthet Dent 2019;121:394-7. https://doi.org/10.1016/j.prosdent.2018.03.018.

[10] Granata S, Giberti L, Vigolo P, Stellini E, Di Fiore A. Incorporating a facial scanner into the digital workflow: A dental technique. J Prosthet Dent 2020;123:781-5. https://doi.org/10.1016/j.prosdent.2019.05.021.

[11] Xiao Z, Liu Z, Gu Y. Integration of digital maxillary dental casts with 3D facial images in orthodontic patients. Angle Orthod 2020;90:397-404. https://doi.org/10.2319/071619-473.1.

[12] Pavlidis G, Koutsoudis A, Arnaoutoglou F, Tsioukas V, Chamzas C. Methods for 3D digitization of cultural heritage. J Cult Herit 2007;8:93-8. https://doi.org/10.1016/j.culher.2006.10.007.

[13] Modabber A, Peters F, Kniha K, Goloborodko E, Ghassemi A, Lethaus B, et al. Evaluation of the accuracy of a mobile and a stationary system for three-dimensional facial scanning. J Craniomaxillofac Surg 2016;44:1719-24. https://doi.org/10.1016/j.jcms.2016.08.008.

[14] Kim AJ, Gu D, Chandiramani R, Linjawi I, Deutsch ICK, Allareddy V, et al. Accuracy and reliability of digital craniofacial measurements using a small-format, handheld 3D camera. Orthod Craniofac Res 2018;21:132-9. https://doi.org/10.1111/ocr.12228.

[15] Verhulst A, Hol M, Vreeken R, Becking A, Ulrich D, Maal T. Three-dimensional imaging of the face: A comparison between three different imaging modalities. Aesthet Surg J 2018;38:579-85. https://doi.org/10.1093/asj/sjx227.

[16] Savoldelli C, Benat G, Castillo L, Chamorey E, Lutz JC. Accuracy, repeatability and reproducibility of a handheld three-dimensional facial imaging device: The Vectra H1. J Stomatol Oral Maxillofac Surg 2019;120:289-96. https://doi.org/10.1016/j.jormas.2019.03.012.

[17] Franco de Sá Gomes C, Libdy MR, Normando D. Scan time, reliability and accuracy of craniofacial measurements using a 3D light scanner. J Oral Biol Craniofac Res 2019;9:331-5. https://doi.org/10.1016/j.jobcr.2019.07.001.

[18] Koban KC, Perko P, Etzel L, Li Z, Schenck TL, Giunta RE. Validation of two handheld devices against a non-portable three-dimensional surface scanner and assessment of potential use for intraoperative facial imaging. J Plast Reconstr Aesthet Surg 2020;73:141-8. https://doi.org/10.1016/j.bjps.2019.07.008.

[19] Revilla-León M, Pérez-Barquero JA, Barmak BA, Agustín-Panadero R, Fernández-Estevan L, Att W. Facial scanning accuracy depending on the alignment algorithm and digitized surface area location: An in vitro study. J Dent 2021;110:103680. https://doi.org/10.1016/j.jdent.2021.103680.

[20] Gallardo YNR, Salazar-Gamarra R, Bohner L, De Oliveira JI, Dib LL, Sesma N. Evaluation of the 3D error of 2 face-scanning systems: An in vitro analysis. J Prosthet Dent. 2021. https://doi.org/10.1016/j.prosdent.2021.06.049.

[21] ISO 5725-1:1994. Accuracy (trueness and precision) of measurement methods and results — Part 1: General principles and definitions. Geneva, Switzerland: International Organization for Standardization; 1994.

https://www.iso.org/standard/11833.html

[22] Flynn C, Taberner AJ, Nielsen PM, Fels S. Simulating the three-dimensional deformation of in vivo facial skin. J Mech Behav Biomed Mater 2013;28:484-94. https://doi.org/10.1016/j.jmbbm.2013.03.004.

Tables

Table 1. Description of the measuring points

Table 2. Specifications of the scanners used for scanning

Table 3. Required time to obtain each image: (a) scanning time, (b) processing time

Table 4. Discrepancies between true measuring values (%)

Table 5. Percentage discrepancy (x) range of all measuring points of each handheld−type scanner (n=33)

Figure legends

Fig. 1 The plaster statues as scanning targets

From left to right: Agrippa, George, and Hermes.

Fig. 2 Location of measuring points

The distance from the nasion (NAS) to each measurement point was calculated.

Fig. 3 Digital impression images of Hermes with and without the texture

Fig. 4 Closeup image around the right eye of Hermes's digital impression image

Fig. 5 Surface deviation color maps of each scanner comparing the high-precision scan data

Fig. 6 Relationship between the length of polygons and trueness of the five hand-held type scanners using box-and-whisker plots

Fig. 7 Relationship between the length of polygons and precision of the five hand-held type scanners using box-and-whisker plots

Figure1

Click here to access/download;Figure;Fig1(600dpi).jpg

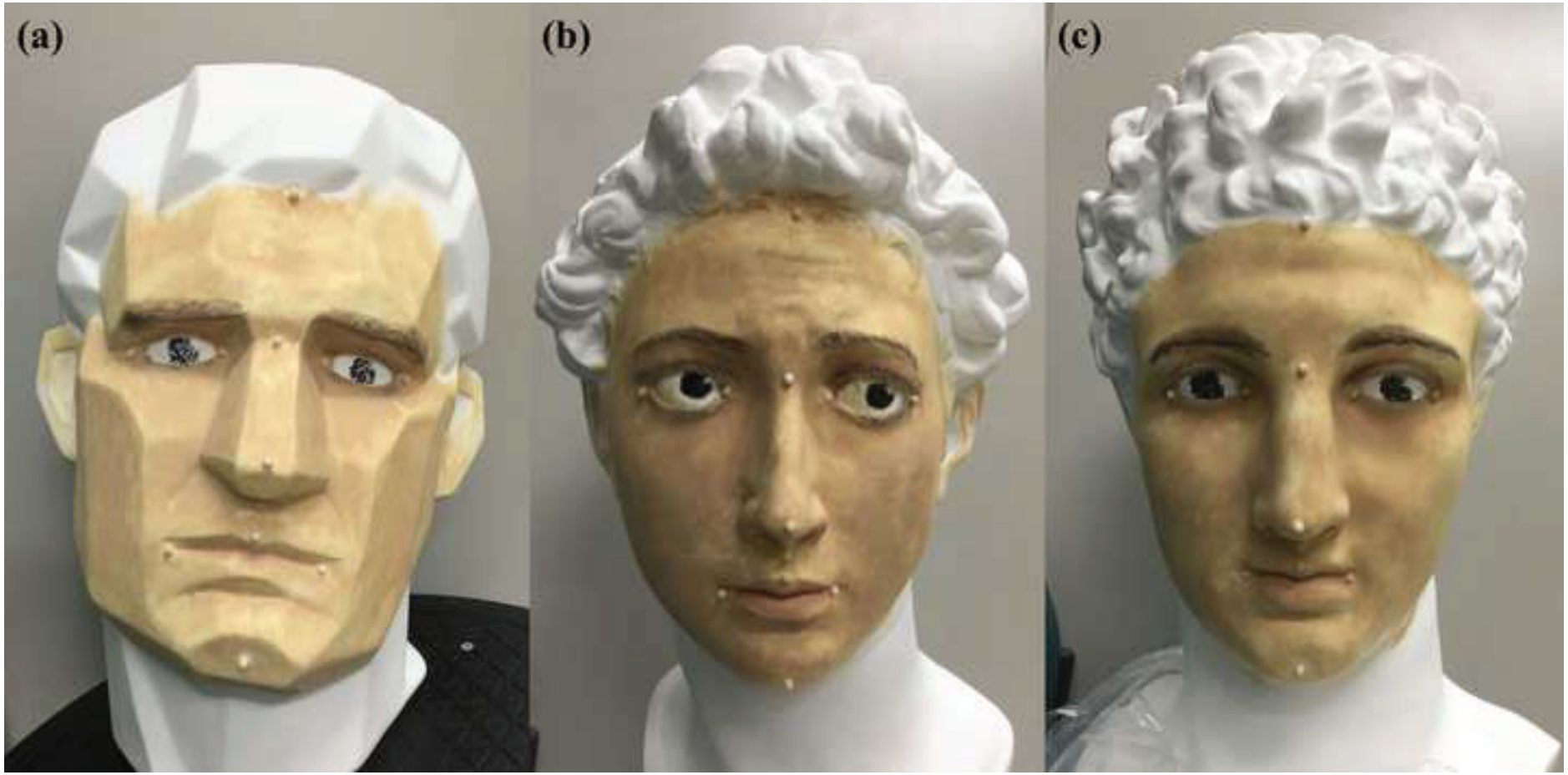

Figure2

Click here to access/download;Figure;Fig2(600dpi).jpg

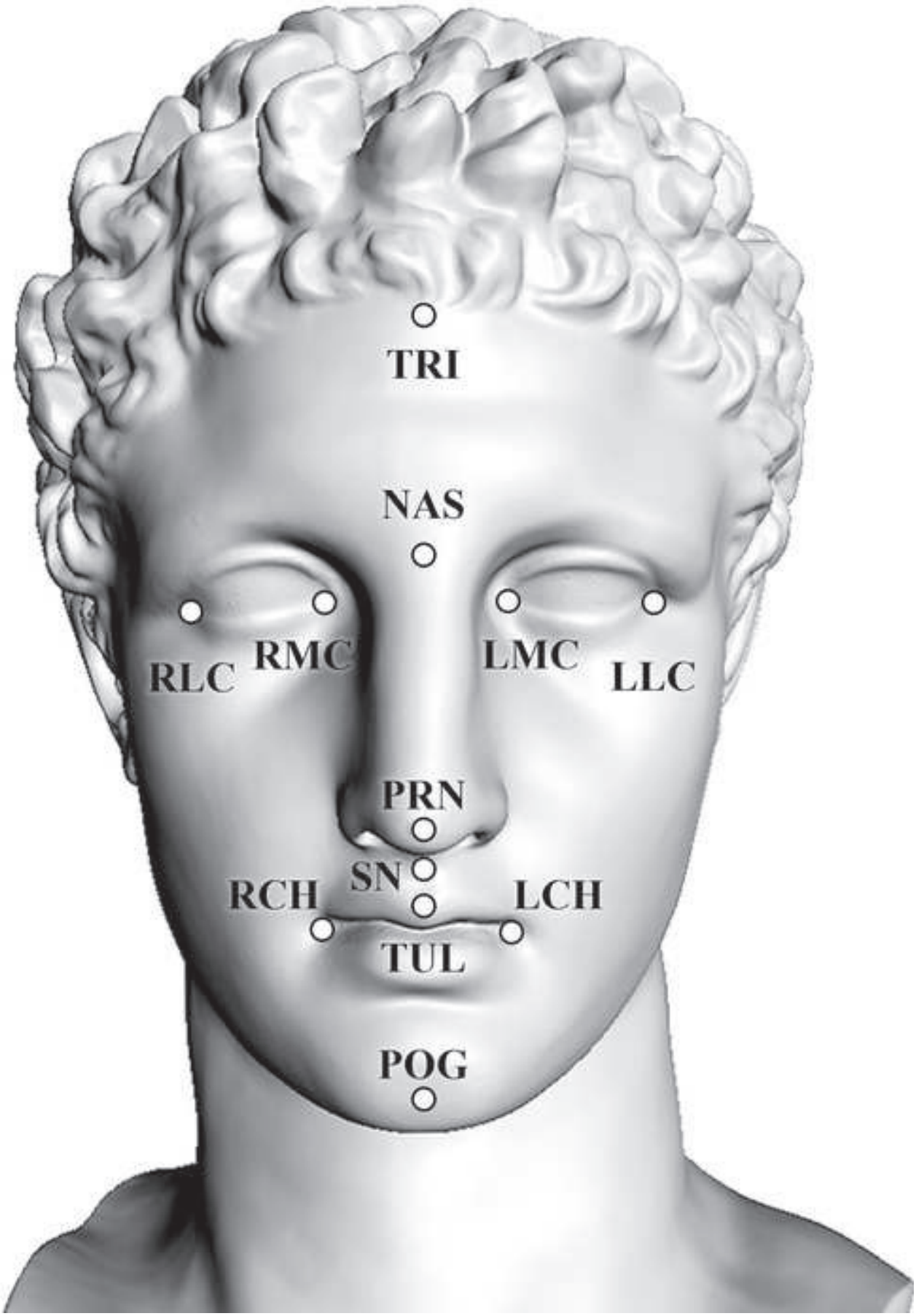

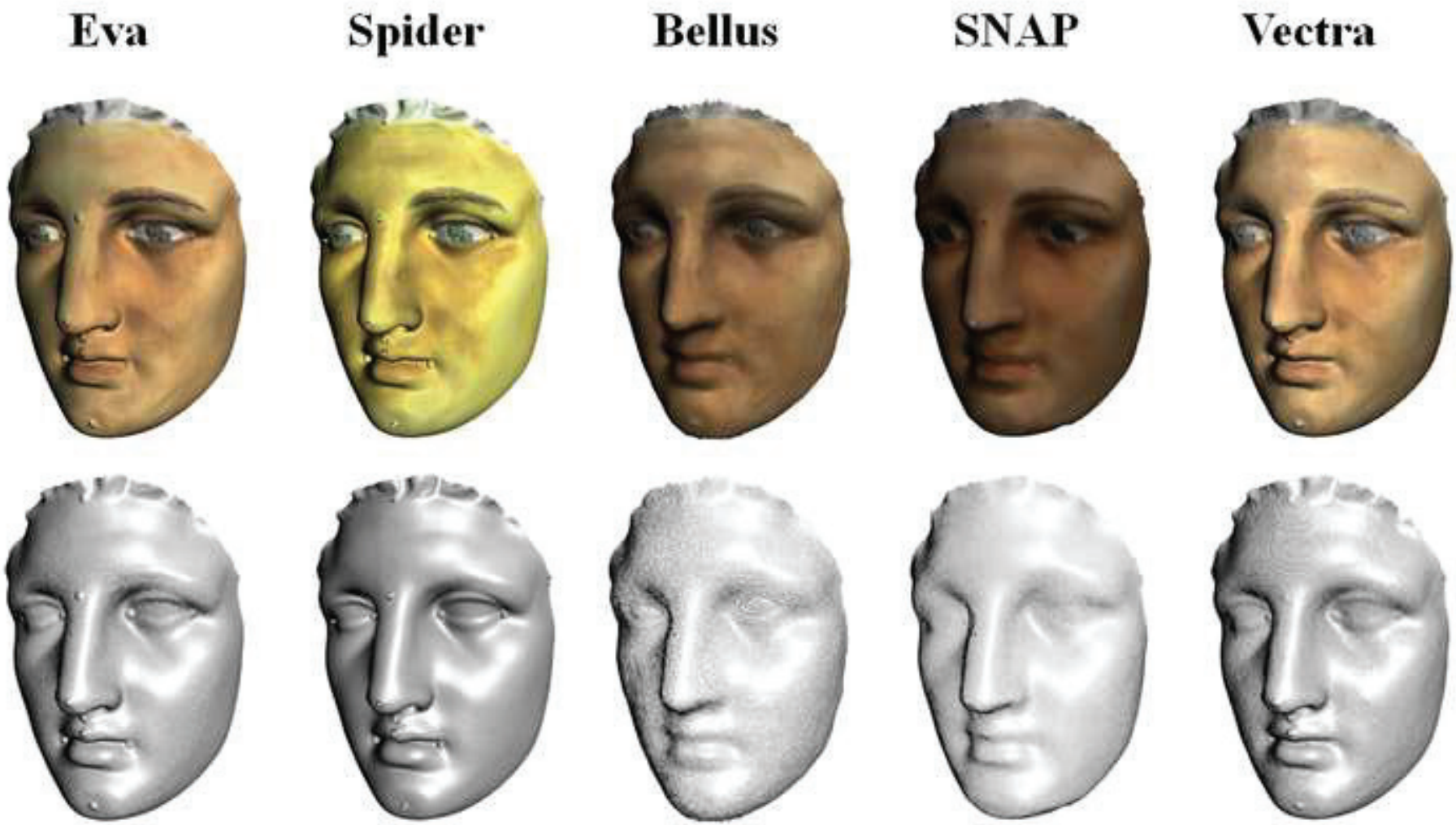

Figure4

Click here to access/download;Figure;Fig4(600dpi).jpg

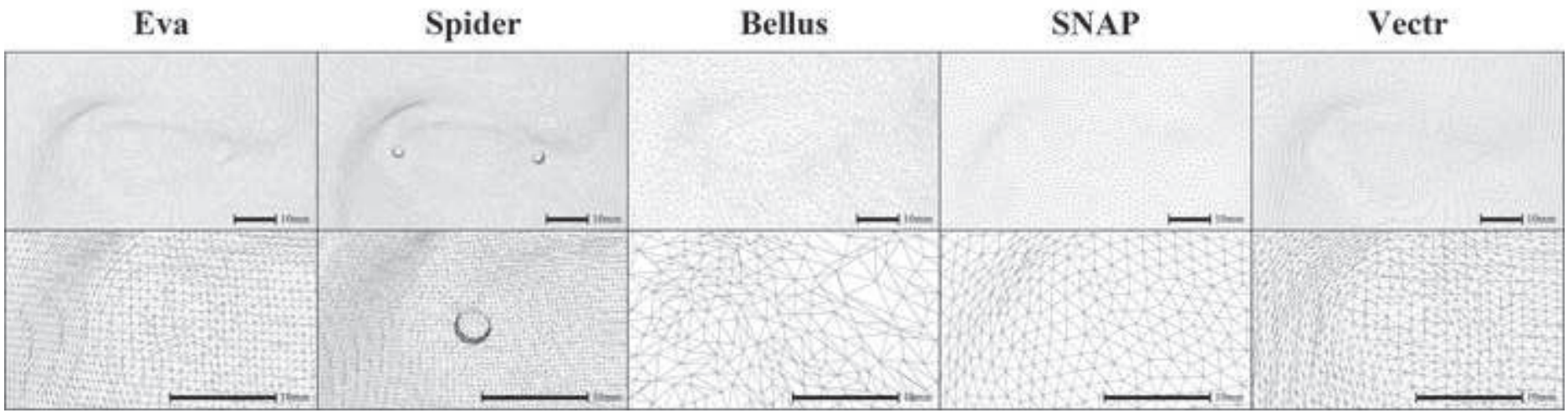

Figure5

Click here to access/download;Figure;Fig5(600dpi).jpg

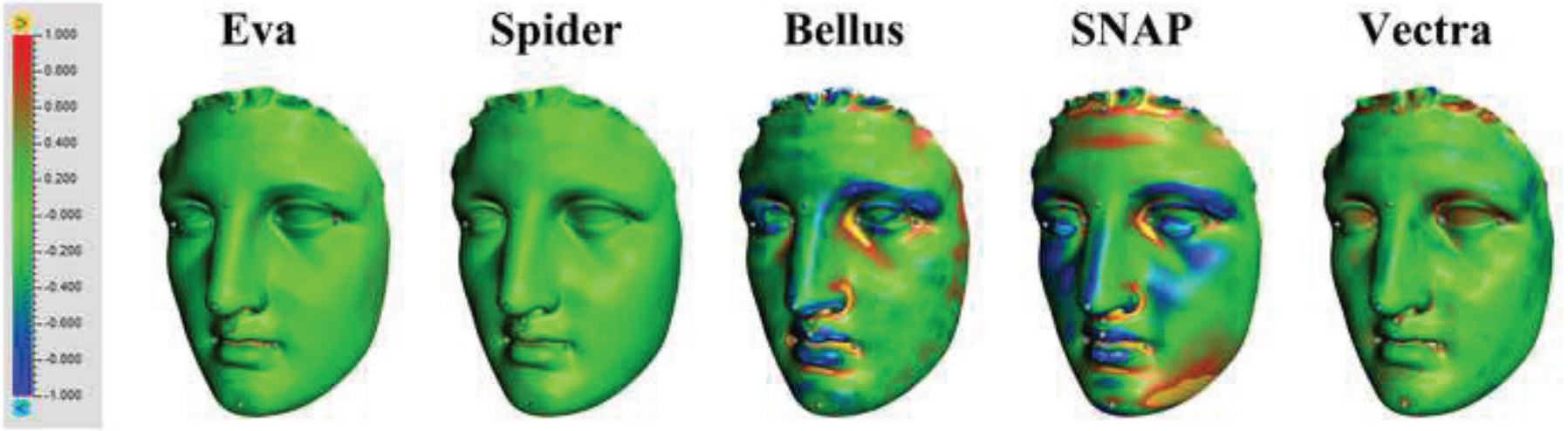

Figure6

Click here to access/download;Figure;Fig6 (600dpi).jpg

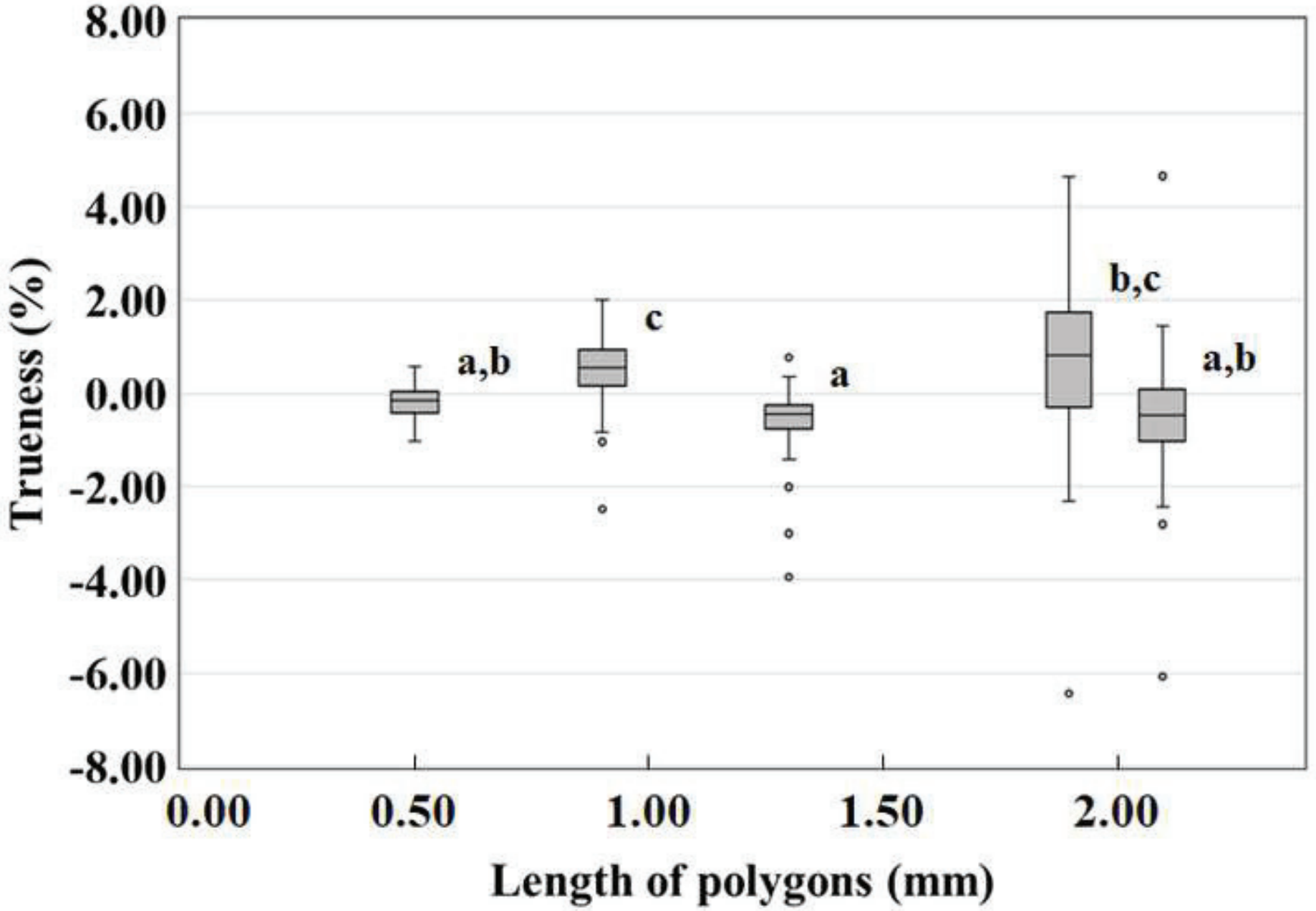

Figure7

Click here to access/download;Figure;Fig7 (600dpi).jpg

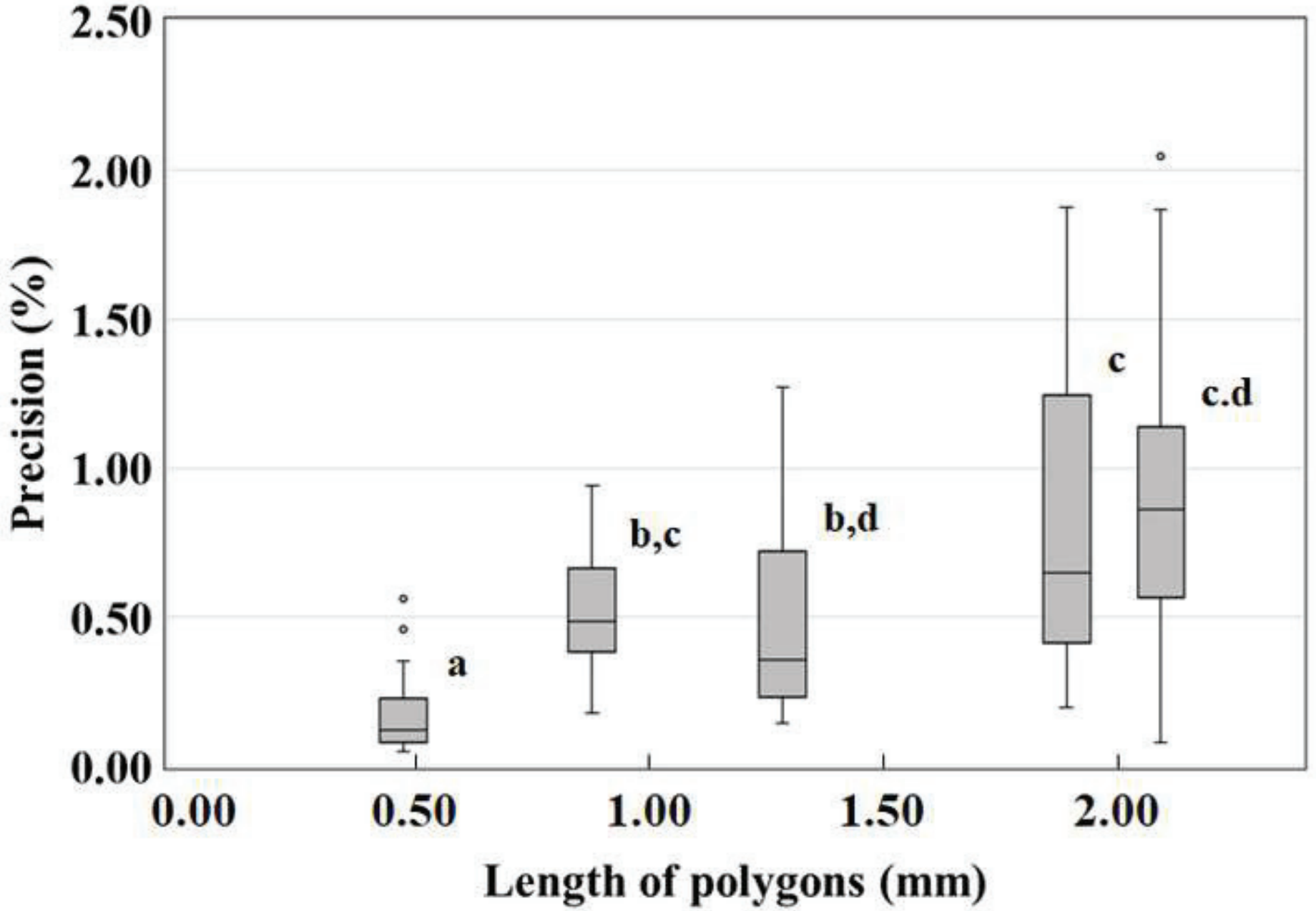

Table 1. Description of the measuring points.

NAS	Nasion	**TRI**	Trichion
PRN	Pronasale	**SN**	Subnasale
TUL	Top upper lip	**POG**	Pogonion
RLC	Right lateral canthus	**LLC**	Left lateral canthus
RMC	Right medial canthus	**LMC**	Left medial canthus
RCH	Right cheilion	**LCH**	Left cheilion

Table 2. Specifications of the scanners used for scanning

	Artec Eva	Artec Spider	Bellus 3D FaceApp	SNAP	Vectra H1
Manufacturer	Artec 3D, Luxembourg	Artec 3D, Luxembourg	Bellus3D, California, US	DOF, Seoul, Korea	Canfield Scientific, New Jersey, US
Measuring device	Special device	Special device	iPhone X (Apple, California, US)	Special device with Surface Pro (Microsoft, Washington, D.C., US)	Special device
Device size (width×depth×height) (mm)	72.0×119.6×222.0	130.0×140.0×190.0	70.9×7.7×143.6	18.0×167.0×17.0	165.0×100.0×270.0
Device weight (g)	850	850	174	840**	N/A
Working range (m)	0.4 – 1.0	0.2 – 0.3	0.3 – 0.45*	0.2 – 1.5	0.45
Light source	LED on device	LED on device	Room light	Room light	On-camera flash
Software	Artec Studio12 Professional	Artec Studio12 Professional	Bellus3D FaceApp Version 1.9.5	DOF SNAP ver 1.4.45.98	Vectra6.5.4
Output file format	obj, ply, wrl, stl, aop, asc, ptx, e57, xyzrgb	obj, ply, wrl, stl, aop, asc, ptx, e57, xyzrgb	stl, obj	obj	stl, obj
Code	Eva	Spider	Bellus	SNAP	Vectra

* Actual measured value
** Including the weight of Surface Pro
N/A: not available

Table 3. Required time to obtain each image: (a) scanning time, (b) processing time.

(a) Scanning time

	Agrippa	George	Hermes
Eva	15.2 ± 1.8 ^{a,A}	16.3 ± 0.8 ^{f,A}	18.3 ± 1.6 ^{i,A}
Spider	42.2 ± 3.3 ^{e,B}	39.8 ± 2.8 ^{h,B}	40.0 ± 2.2 ^{k,B}
Bellus	20.7 ± 0.5 ^{b,C}	20.8 ± 0.4 ^{f,C}	19.5 ± 3.0 ^{i,C}
SNAP	31.0 ± 3.1 ^{d,D}	33.3 ± 4.6 ^{g,D}	38.8 ± 2.2 ^{k,E}
Vectra	26.3 ± 2.5 ^{c,F}	36.8 ± 1.9 ^{gh,H}	32.3 ± 5.1 ^{j,G}

(b) Processing time

	Agrippa	George	Hermes
Eva	124.0 ± 5.7 ^{c,B}	89.3 ± 6.3 ^{f,A}	116.8 ± 22.8 ^{k,B}
Spider	234.2 ± 12.3 ^{d,E}	147.3 ± 11.9 ^{h,C}	175.5 ± 8.3 ^{l,D}
Bellus	23.5 ± 2.3 ^{a,F}	20.7 ± 2.7 ^{e,F}	21.7 ± 3.7 ^{i,F}
SNAP	71.7 ± 11.1 ^{b,G}	77.2 ± 14.2 ^{f,G}	96.7 ± 7.7 ^{j,H}
Vectra	116.0 ± 7.0 ^{c,I}	112.2 ± 7.0 ^{g,I}	122.0 ± 4.9 ^{k,I}

Values with the same upper-case letter are not significantly different among statues.

Values with the same lower-case letter are not significantly different among scanners.

Table 4. Discrepancies between true measuring values (%).

		True Value (mm)	Eva				Spider				Bellus				SNAP				Vectra			
(a) Agrippa	**TRI**	63.49	0.59	±	0.57	bc, A	0.02	±	0.20	d, A	−0.42	±	0.72	efg, A	0.45	±	0.51	jklm, A	−0.30	±	0.61	op, A
Vertical	**PRN**	53.56	−1.04	±	0.56	a, BCD	−0.17	±	0.13	d, D	−1.23	±	1.43	e, BC	−1.94	±	0.65	i, B	−0.77	±	0.89	o, CD
	SN	66.96	1.45	±	0.70	c, F	−0.45	±	0.14	d, E	4.66	±	1.87	h, H	3.20	±	1.25	n, G	0.87	±	0.39	p, EF
	TUL	79.83	−0.73	±	0.45	ab, I	−0.35	±	0.09	d, I	−0.06	±	0.60	efg, I	1.42	±	0.89	klm, J	−0.63	±	0.22	o, I
	POG	131.41	0.39	±	0.33	bc, K	−0.20	±	0.05	d, K	0.29	±	0.62	g, K	0.15	±	0.61	jk, K	−0.45	±	0.36	op, K
Horizontal	**RLC**	70.84	1.22	±	0.42	c, N	−0.42	±	0.14	d, LM	−1.40	±	0.50	e, L	0.03	±	0.93	j, M	−1.01	±	0.36	o, LM
	LLC	71.35	0.95	±	0.20	c, Q	−0.09	±	0.14	d, OP	−1.13	±	1.16	ef, O	0.32	±	0.78	jkl, PQ	−0.33	±	0.88	op, OP
	RMC	32.17	0.42	±	0.94	bc, S	−0.46	±	0.21	d, RS	−0.39	±	0.88	efg, RS	−0.27	±	0.47	j, RS	−1.05	±	0.77	o, R
	LMC	33.56	0.54	±	0.73	bc, TU	0.03	±	0.35	d, T	0.37	±	1.41	g, T	1.58	±	1.08	lm, U	0.07	±	1.27	op, T
	RCH	98.05	0.56	±	0.41	bc, V	−0.15	±	0.09	d, V	0.14	±	0.53	fg, V	1.72	±	0.64	m, W	−0.33	±	0.31	op, V
	LCH	97.12	0.34	±	0.63	bc, XY	−0.09	±	0.11	d, X	−0.31	±	0.33	efg, X	0.89	±	0.59	jklm, Y	−0.24	±	0.23	op, XY

Values with the same upper-case letter are not significantly different among scanners.

Values with the same lower-case letter are not significantly different among the measuring points.

		True Value (mm)	Eva				Spider				Bellus				SNAP				Vectra			
(b) George	**TRI**	66.85	1.09	±	0.65	e,	B	0.04	±	0.30	f,	A	−0.66	±	1.06	i,	A	2.09	±	0.34	n,	C	−0.73	±	0.37	q,	A
Vertical	**PRN**	58.44	−0.83	±	0.68	b,	D	−0.35	±	0.14	f,	D	−0.82	±	0.38	i,	D	−0.72	±	0.24	l,	D	−0.64	±	0.72	q,	D
	SN	69.32	0.19	±	0.84	bcde,	EF	−0.39	±	0.08	f,	E	0.30	±	1.00	i,	EF	0.80	±	0.61	m,	F	−0.24	±	0.65	q,	E
	TUL	78.57	−0.22	±	0.44	bcd,	G	−0.42	±	0.12	f,	G	−0.36	±	0.08	i,	G	1.25	±	0.20	mn,	H	−0.59	±	0.15	q,	G
	POG	128.57	0.21	±	0.45	bcde,	IJ	−0.26	±	0.10	f,	I	0.04	±	0.82	i,	IJ	0.93	±	0.23	m,	J	−0.50	±	0.28	q,	I
Horizontal	**RLC**	67.11	1.21	±	0.49	e,	L	−0.63	±	0.25	f,	K	−0.80	±	0.40	i,	K	4.03	±	0.32	o,	M	−0.05	±	0.35	q,	K
	LLC	63.29	0.83	±	0.46	de,	OP	−0.02	±	0.26	f,	NO	−0.68	±	0.88	i,	N	1.76	±	0.61	mn,	P	−0.43	±	0.72	q,	N
	RMC	33.10	−0.51	±	0.58	bc,	R	−0.92	±	0.46	f,	R	−2.44	±	1.52	h,	Q	−2.32	±	0.60	k,	Q	−3.01	±	1.05	p,	Q
	LMC	29.53	−2.49	±	0.48	a,	U	−0.87	±	0.56	f,	V	−6.08	±	0.86	g,	S	−6.44	±	1.24	j,	S	−3.93	±	1.14	p,	T
	RCH	95.69	0.45	±	0.39	cde,	X	−0.45	±	0.08	f,	WX	−0.58	±	0.22	i,	W	1.93	±	0.35	mn,	Y	−0.48	±	0.16	q,	WX
	LCH	92.64	0.61	±	0.49	cde,	αβ	−0.39	±	0.08	f,	Z	−0.31	±	0.34	i,	Zα	1.37	±	0.24	mn,	β	−0.54	±	0.25	q,	Z

Values with the same upper-case letter are not significantly different among scanners.

Values with the same lower-case letter are not significantly different among the measuring points.

		True Value (mm)	Eva					Spider					Bellus					SNAP					Vectra				
(c) Hermes	**TRI**	59.06	−0.61	±	0.75	a,	A	−1.03	±	0.31	d,	A	−1.75	±	0.85	efg,	A	−0.43	±	1.14	jk,	A	−1.43	±	0.14	pq,	A
Vertical	**PRN**	62.97	1.34	±	0.91	bc,	C	0.56	±	0.07	d,	BC	−0.48	±	1.44	gh,	B	−0.35	±	1.87	jk,	B	0.21	±	0.31	qr,	BC
	SN	73.94	2.01	±	0.60	c,	E	0.51	±	0.11	d,	D	1.45	±	1.33	i,	DE	0.46	±	1.70	klm,	D	0.76	±	0.44	r,	DE
	TUL	82.21	0.60	±	0.38	abc,	F	0.20	±	0.06	d,	F	0.66	±	0.90	hi,	F	2.30	±	1.85	n,	G	−0.13	±	0.19	qr,	F
	POG	131.94	0.59	±	0.22	abc,	HI	0.22	±	0.05	d,	HI	0.45	±	0.71	hi,	HI	1.59	±	1.44	lmn,	I	−0.28	±	0.17	qr,	H
Horizontal	**RLC**	69.20	1.51	±	0.18	bc,	KL	−0.14	±	0.28	d,	J	−0.41	±	0.76	gh,	J	2.09	±	1.25	mn,	L	0.35	±	0.49	r,	JK
	LLC	73.45	0.94	±	0.35	abc,	N	−0.20	±	0.12	d,	MN	−0.94	±	1.11	fgh,	M	4.66	±	0.20	o,	O	−0.69	±	0.27	pqr,	M
	RMC	39.58	0.14	±	0.93	ab,	Q	0.21	±	0.20	d,	Q	−2.16	±	1.04	ef,	P	−1.70	±	1.24	j,	P	−1.34	±	0.62	pq,	P
	LMC	38.51	0.44	±	0.61	abc,	U	−0.03	±	0.12	d,	TU	−2.82	±	2.05	e,	R	−1.06	±	0.92	jk,	ST	−2.01	±	0.84	p,	RS
	RCH	98.60	0.83	±	0.18	abc,	W	0.31	±	0.06	d,	VW	−0.75	±	1.05	fgh,	V	−0.17	±	1.28	jk,	VW	−0.38	±	0.17	pqr,	VW
	LCH	98.06	0.89	±	0.29	abc,	Y	0.17	±	0.05	d,	XY	−0.76	±	0.77	fgh,	X	0.01	±	1.32	kl,	XY	−0.44	±	0.23	pqr,	XY

Values with the same upper-case letter are not significantly different among scanners.

Values with the same lower-case letter are not significantly different among the measuring points.

Table 5. Percentage discrepancy (x) range of all measuring points of each handheld−type scanner (n=33).

	Eva	Spider	Bellus	SNAP	Vectra
$3.00 \leq x$	0	0	1	3	0
$2.00 \leq x <$ 3.00%	1	0	0	3	0
$1.00 \leq x <$ 2.00%	6	0	1	8	0
$0.00 \leq x <$ 1.00%	19	10	7	9	5
$-1.00 \leq x <$ 0.00%	5	22	16	5	21
$-2.00 \leq x <$ −1.00%	1	1	4	3	4
$-3.00 \leq x <$ −2.00%	1	0	3	1	1
$x <$ −3.00%	0	0	1	1	2